Nuclear Inst. and Methods in Physics Research, A 983 (2020) 164588

Contents lists available at ScienceDirect

Nuclear Inst. and Methods in Physics Research, A

journal homepage: www.elsevier.com/locate/nima

GaToroid: A novel toroidal gantry for hadron therapy

L. Bottura [a,*], E. Felcini [a,b], G. De Rijk [a], B. Dutoit [b]

[a] TE Department - CERN, 1211 Geneva 23, Switzerland
[b] Groupe SCI IC BD-EPFL, 1015, Lausanne, Switzerland

ARTICLE INFO

Keywords:
Hadron therapy
Gantry
Toroidal magnet
Superconducting magnet

ABSTRACT

We describe here a novel concept of a gantry for hadron therapy, based on the use of a toroidal field configuration. The main features of this concept are that the gantry is not rotating, and is operated in steady-state We propose that is built based on superconducting magnets, reaching field levels not achievable using normal conducting iron-dominated magnets. The simplification resulting from the specific magnetic configuration, and the scale reduction that can be achieved using high-field superconducting magnets, bear a definite potential for significant reduction of dimensions and mass. In this paper we introduce the concept of the toroidal gantry, discussing the features of beam transport in a toroidal field. We then provide general considerations on the design of the coil, and analytical scaling of relevant indicators such as forces and stored energy. Finally, we give an example of practical layouts for a proton gantry that can be used as a benchmark for comparison with other designs.

1. Introduction

Hadron therapy refers to a medical treatment technique that uses hadron beams (i.e. protons and ions), profiting from the Bragg peak to deliver localized energy that suppresses cancerous cells, sparing the neighboring healthy tissues from unwanted radiation. Hadron therapy centers, and especially those based on ion beams, tend to be relatively large, complex and costly installations. This is why, in spite of the potential benefits [1–5], the penetration of this medical technology is still limited. Several initiatives, past, present and future, are dedicated to reducing the size and cost of the accelerator [6,7], that is the first key element and cost driver of a hadron therapy center. Beam delivery, which is the focus of this paper, is the second key element of the installation [8–10], and also a significant cost driver [11].

In general, the beam delivery itself can consist of one or more fixed transfer lines [12], or it can include a *gantry*, a transfer line mounted on a large mechanical structure that rotates around the patient and allows radiation from multiple directions [13].

The magnets of a gantry are required to rotate with high precision, which results in massive mechanical structures. In addition, the field produced by the gantry magnets needs to be variable to some degree, as the magnet bore size alone does not allow accepting the desired full energy range.

While gantries for protons are relatively widespread, gantries for ions, requiring the largest magnets, remain a spectacular engineering feat. Only two such gantries have been built and are operating to date. The one hosted at the Heidelberg Ion Therapy (HIT) Center is based on resistive magnets, and entails a structure of 14 meters in diameter, 22 m in length, and more than 600 tons of weight [14]. A second gantry for ions is in use at the Heavy Ion Medical Accelerator in Chiba (HIMAC), based on Nb–Ti combined functions superconducting magnets, and has an outer diameter of 9 m, a length of 13 m and a mass of approximately 300 tons [15].

The social and commercial opportunity, and the technological challenge have motivated a number of studies of different and optimized solutions for ion gantries. Alternative transfer line designs have been considered, to increase acceptance and avoid ramping the magnets [16,17], or to reduce the lattice dimensions by using combined function magnets [18–20]. Weight reduction has been pursued by using toroidal magnets, exploiting the flux return properties to reduce the mass of a rotating gantry [21]. A completely different configuration, consisting of a structure that rotates the patient room around a rotating bending magnet, was studied up to the conceptual design level [22]. In any of these solutions, the concept entails a rotating transfer line and a heavy mechanical structure. Finally, a relevant example in the context of this manuscript is the *Piotron*, built at PSI in 1980, where tori of superconducting coils were used to focus pions for therapy [23,24].

In this paper we present a new configuration for the beam delivery system, based on a steady-state, axis-symmetric field configuration. The basic idea is to use fixed *toroidal magnets*, producing the axis-symmetric (or periodical axis-symmetric) field configuration that can bend beams from several directions onto the patient location. In principle, neither magnets nor patient need to be moved. In addition, the field of the

* Corresponding author.
E-mail address: Luca.Bottura@cern.ch (L. Bottura).

https://doi.org/10.1016/j.nima.2020.164588
Received 28 February 2020; Received in revised form 31 July 2020; Accepted 25 August 2020
Available online 28 August 2020

magnets of this *toroidal gantry* is static. A single upstream *vector magnet* provides the beam steering, which depends on the beam energy and direction of irradiation.

The system we propose has several advantages. The first benefit is that the mechanical structure of the steady and axis-symmetric configuration is much simpler and lighter than a rotating gantry. The magnet is fixed in space and operates in steady state, so it is appropriate to conceive the use of superconducting materials for the toroidal magnet, generating significantly higher field than existing normal-conducting solutions. This has the further potential of a very significant reduction of the footprint. Last but not least, the steady state nature of the gantry would allow simultaneous irradiations from different directions at different energies, with the only limitation imposed by the ability of the accelerator to deliver such beams, and the vector magnet to follow the desired changes.

Below we detail the concept of such system, its basic properties, configuration and possible alternatives. We start with the basic beam transfer properties of toroidal fields, and then describe the concept of the toroidal gantry system. We further develop on specific features that are important to the implementation of the concept, such as coil geometry, grading and axial symmetry. We finally give an example of a compact design, based on requirements applicable to proton therapy. The intention of this paper is to document the concept and identify the main features and issues. We defer to later work the engineering design of the system, including matters of beam dynamics [25] and actual implementation in a therapy center.

2. Beams in ideal toroidal fields

To discuss the effect of toroidal field on beams we consider here the ideal, axis-symmetric field generated by a thin toroidal current winding. We define the symmetry axis of the torus to be the z direction. The field inside the torus is directed along the angle θ, and normal to the radius R, measured from the axis of the toroid (standard cylindrical coordinates convention is used). The ideal field has module given by:

$$B_\theta = \frac{B_{ref} R_{ref}}{R} \tag{1}$$

where B_{ref} and R_{ref} are constants determined by the location and intensity of the current in the winding. B_{ref} is a *reference field*, at radius R_{ref}. The field is zero outside the toroidal winding.

We now consider a single particle traveling in the (R, z) plane, at an arbitrary angle θ, entering the region of toroidal field, and neglect the presence of the toroidal winding. By pure intuitive considerations, we see that the toroidal field (with correct polarity and strength) will bend the particle towards its axis, irrespective of the angle θ. The kick seen by the particle will depend on the integrated field strength, i.e. the field intensity and dimension of the toroidal winding. The effect of a toroidal field is hence to *focus* single particles traversing the field region towards the axis of symmetry.[1]

To develop further on this property, and provide a quantitative demonstration, we take some simple limiting cases. We consider first that the ideal toroidal field covers a rectangular region of space $z_{\min} < z < z_{\max}$ and $R > R_0$, and limit the discussion to a particles of charge q entering the toroidal field area with momentum p in the (R, z) plane. The field is generated by a thin and immaterial sheet of current. The particle trajectory can be tracked using the simple relation:

$$B_\theta \rho = \frac{p}{q} \tag{2}$$

where ρ is the curvature radius in the (R, z) plane. The momentum is defined using the relativistic relation:

$$p = E_0 \sqrt{\gamma^2 - 1} \tag{3}$$

[1] Note that the *focusing* effect quoted here refers to the fact that the toroidal field causes a convergence of the single particles towards the axis of the toroid. Focusing in the sense of beam dynamics, and more in general matters of beam optics in a toroidal field are described in a companion paper [25].

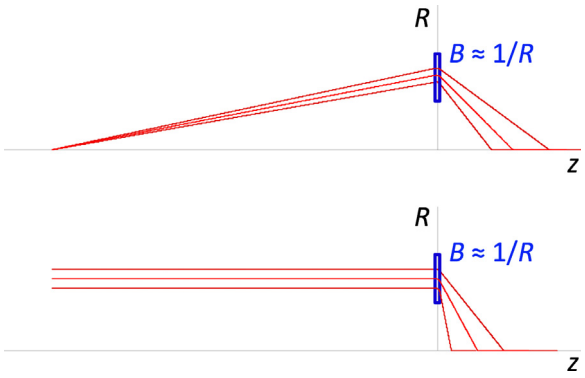

Fig. 1. Effect of a thin toroidal field lens on particles with the same momentum, traveling in the (R, z) plane, either parallel to each other (top), or originating at the same vertex but diverging (bottom). The current sheet is represented by the rectangular contour. Ideal toroidal field with $1/R$ dependency. The effect of the lens is a net convergence (*focusing*) with a strong astigmatic error.

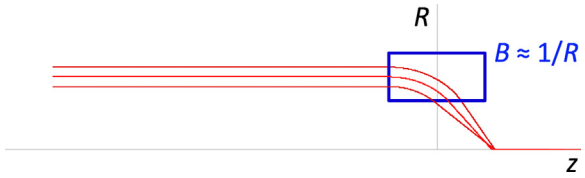

Fig. 2. Effect of a thick toroidal field lens on particles with the same momentum, traveling in the (R, z) plane, parallel to each other. Ideal toroidal field with $1/R$ dependency. The effect of the thick lens is a net convergence (*focusing*) with a much reduced astigmatic error.

where E_0 is the rest energy of the particle (or ion) considered, and γ is the relativistic factor:

$$\gamma = 1 + \frac{E_K}{E_0} \tag{4}$$

defined by the kinetic energy E_K of the particle.

If the toroidal field magnet is *short* in z direction, i.e. what we can call the equivalent of a *thin toroidal lens*, the *focusing* effect is demonstrated in Fig. 1 for two possible situations: particles of identical momentum, either traveling along the z-axis and parallel to each other, or originating at a vertex located at the z-axis. The thin toroidal lens has indeed the expected net convergent effect towards the z-axis, but the $1/R$ dependence of the ideal toroidal field on the radius results in a strong *astigmatism* because the outer particles are bent less than the inner ones.

Let us consider now a toroidal magnet with dimension comparable to the variation of the particle orbit (i.e. a *thick toroidal lens*), and we notice that the astigmatism is much reduced. This effect is shown schematically in Fig. 2, where again the tracks correspond to particles with the same momentum. The reduced astigmatism is due to the fact that particles entering with large orbit (or large angle) travel a longer path in the field than particles entering at small orbit or angle, thus resulting in additional *focusing*. Note that here no special effort is made to achieve particle convergence in a single point, besides a choice of energy, field and coil dimensions that demonstrates the effect.

We then examine the case of particles of different momentum (or more in general p/q ratio) originating at the same vertex. This is shown schematically in Fig. 3, where now tracks correspond to particles with the same angle, and a variation of p/q by a factor two, i.e. relevant to our discussion. As expected, particles with higher rigidity are bent less. However, taking into account the observation above on the focusing effect of the length traveled in the field region, it is possible to find appropriate initial angles for each of the beams in the selected range such that the focal point on the z-axis is the same for all values of p/q.

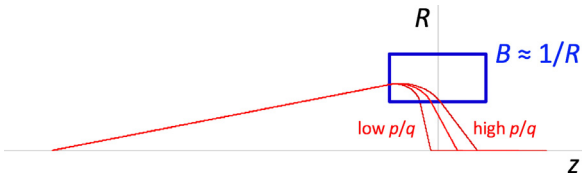

Fig. 3. Effect of a thick toroidal field lens on particles with different p/q, differing by a factor 2, originating at the same vertex on the z-axis and with the same initial direction. Ideal toroidal field with $1/R$ dependency. The particles converge on the at different points on the z-axis depending on their p/q ratio, beams with higher momentum traveling to farther distances.

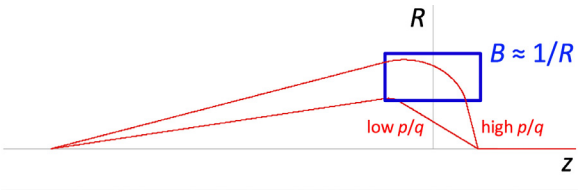

Fig. 4. A possible compensation of the effect shown in Fig. 3. Particles with different p/q, differing by the same factor 2 as in Fig. 3, and originating at the same vertex, are given different initial directions so that they travel in the thick toroidal lens over different path lengths. Ideal toroidal field with $1/R$ dependency. The net effect is to converge the different particles in the same point on the z-axis.

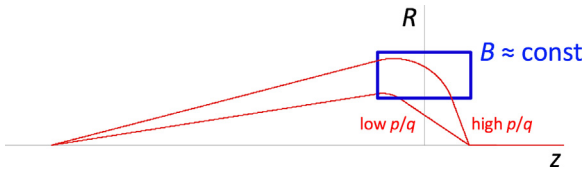

Fig. 5. Same simulation as in Fig. 4, but taking a constant toroidal field in the coil space (field index $n = 0$). The single particles converge as observed in Fig. 4, but the in-field path of the low momentum particle is much longer.

This is finally demonstrated in Fig. 4, where the particles of different p/q are kicked by different amounts at the common vertex, enter the thick toroidal lens in different points, and converge to the same focal point on the z-axis. The higher momentum particle is kicked by a larger angle, and travels a longer path compared to the smaller momentum particle, which is kicked by a smaller angle and travels a shorter path in the field. Convergence to the single point was obtained by a trial-end-error sequence of tracking, achieving any desired (numerical) accuracy on the z-axis.

So far we have considered in our demonstration a toroidal field with the natural $1/R$ dependency. As shown in Fig. 4 such arrangement causes the particles of low momentum, kicked at a lower angle, to experience a larger field than particles with higher momentum. The path of the low momentum particle can be very short, and make the system very sensitive to small errors. This can be improved by introducing a radial field index n such that the toroidal field is given by:

$$B_\theta = \frac{B_{ref} R_{ref}^n}{R^n} \tag{5}$$

Eq. (5) is a modified form of Eq. (1), and indicates that the field can deviate from the ideal $1/R$ dependency of the toroid with infinitesimally thin winding considered so far. This can is achieved *grading* the coil winding of the toroid, as we will explain later in Section 3.2.2.

A convenient choice of the field index is $n = 0$, i.e. a constant toroidal field in the space of the coils. The effect of this choice is shown in Fig. 5, where we take the same conditions of Fig. 4, i.e. a factor 2 in the p/q ratio of two particles, but the field is now constant. The length traveled by the low energy particle is now more than doubled, making the system considerably less critical to small adjustments in the kick angle.

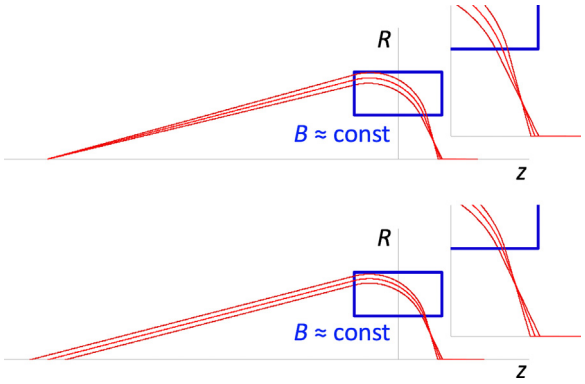

Fig. 6. Effect of small angular kicks around a reference direction for particles with equal p/q, and originating at the same vertex (top), or with identical angular kick but originating at shifted vertex points (bottom). Constant toroidal field in the coil space (field index $n = 0$). The particles arrive at the z-axis with a longitudinal shift, as shown in the detail. This effect can be used to *paint* a desired area with particles of a given p/q.

Finally, we demonstrate the effect of small deviations from the reference direction, as well as changes in the location of longitudinal magnetic center of the vector magnet. This is shown in Fig. 6, where the upper momentum of Fig. 5 has been taken as a reference, and two particles are traced with initial direction slightly differing from the reference, or with a small shift of the vertex location along the z-axis. The effect is a movement of the focal point, also by a small amount. This indicates that location and direction of the particle at the vertex must be precise to direct particles as desired on the toroid axis. At the same time this feature can be exploited to *paint* a region around the nominal focus of the toroidal field.

So far all analyses were assuming a particle traveling in the (R, z) plane. Without entering in the details of 3D tracking, developed elsewhere [25], we simply note that a particle with out-of-plane momentum will experience a centering force that depends on the curvature of the field. This is similar to the effect of field curvature in a combined function magnet.

In summary, a toroidal field of appropriate polarity can act as a convergent lens for particles of different direction and momentum. The focal point of the lens depends on the field strength and geometry, affecting the length of the particle path in the toroidal field area. It is in principle possible to *focus* particles of different p/q ratio in the same point by actively directing them in different regions of the toroid. Changing the initial direction of particles of identical p/q ratio, the point where the axis is crossed moves. These are the properties that are at the basis of our novel gantry configuration, described in the next section. We will further develop features such as coil shaping, winding grading, finite coils, and periodic angular spacing (parallel channels) that are necessary to make the concept practical.

3. Concept of the gantry system

The concept of the system proposed is rendered in Fig. 7 [26], and it consists of two main parts that realize the basic idea described in the previous section:

- A vector magnet, receiving beam from the accelerator extraction line, and providing a kick that depends on the energy of the beam and the desired direction of beam delivery;
- One or more co-axial toroidal magnets (one magnet only is depicted in Fig. 7 as an example), that bend the beam by using a combination of their shape and field variation with radius and length.

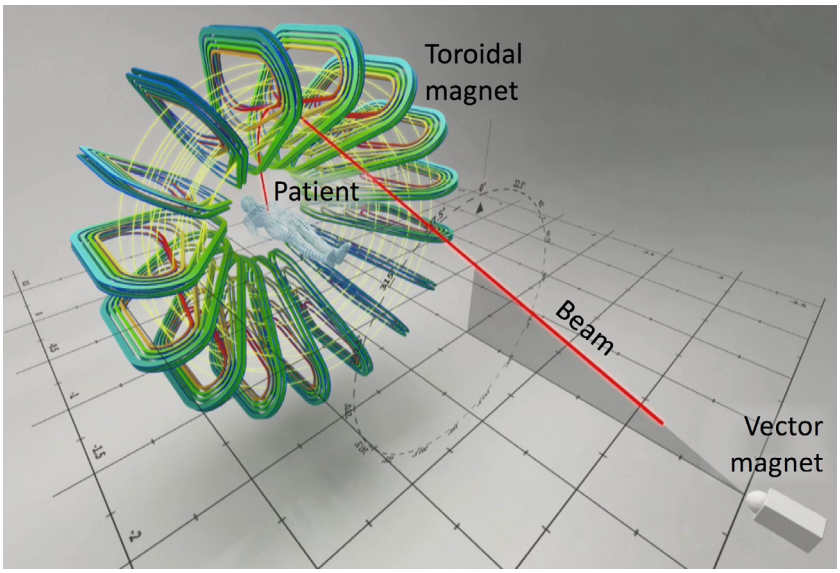

Fig. 7. Schematic representation of the components and functions in the toroidal gantry, with a beam trajectory, of a given energy, demonstrating the drift and bend. The vector magnet is represented as a single unit that can kick in any direction, while the toroidal gantry consists in this case of a single toroidal magnet. The patient is located in the (field-)free bore of the toroidal magnet (courtesy of Daniel Dominguez, CERN Design and Visual Identity Service).

The patient is placed in the axis of the toroid. Each part is described in more detail in the sections below. The main focus in this paper is on the toroidal magnet, the true novelty of the concept.

3.1. Vector magnet

The function of the *vector magnet* is to bend the extracted beam in any direction by an angle that depends on the beam energy. For a given energy, this corresponds to the ability to produce a cone of beam trajectories originating at the location of the vector magnet.

To achieve this function, the vector magnet can be a single dipole rotating around its axis with the ability to sweep the field strength. Depending on the magnet design, the change in field strength required to steer beams of different energy can be relatively fast. A rotation, on the other hand, corresponding to a change in irradiation direction, will be much slower. An alternative to achieve fast response in both functions is to consider a two-axis vector magnet, producing a combination of horizontal and vertical dipole with arbitrary direction. In this case the two dipoles should change setting frequently, providing the ability for rapid energy and direction changes, and eliminating the need for a heavy rotating machinery. This feature makes the two-axis option more elegant and interesting.

In addition to the momentum-dependent kick, the vector magnet can act with deviations from the nominal kick to achieve the beam spot scanning that is requested in hadron therapy. This is conceptually identical to the ability to kick in an arbitrary direction described above, albeit by a much smaller amount.

We are aware that the vector magnet poses by itself a significant technology challenge. An ideal vector magnet should be short, to keep the aperture at the exit small, but sufficiently strong to avoid a large distance from the vertex to the toroid. This would result in relatively large fields (e.g. in excess of 3 T), i.e. calling for a superconducting solution. In this case the associated inductance and inevitable AC loss would pose a limit to ramping speed, thus contradicting the desire to achieve fast switching. Accuracy in the X-Y kick is of paramount importance, to direct particles at the desired location. This should be true both for the large steps that cover the desired range of momentum (i.e. an approximate factor of three in the kick), as well as the small sweeps used to paint the desired region (i.e. order of few percent in the kick).

Without entering in the details of the design of a two-axis vector magnet, we note that the functions described above do not need to be realized with a single component. Indeed, the most convenient realization of a vector magnet is a sequence of magnets with separate functions (e.g. energy bend, angular bend, steerer for painting). In fact, a combination of a resistive X-Y fast switching magnet followed by a large aperture superconducting bend (a *forward* toroid) could provide the best combination of features. Work on this part of the system is in progress and will be reported separately.

3.2. Toroidal gantry

The gantry proper consists of a set of co-axial toroids, with identical z-axis. Each toroidal magnet is made of N discrete coils, generating the desired field. Only the space between two neighboring coils is free for the beam passage, so that the coil geometry defines N *beam channels* that have an equivalent bending function. The toroidal gantry has hence the particularity that it can only deliver beams at discrete angular locations. A study of the statistics of beam delivery directions in actual treatment plans has shown that the majority of beam is delivered only at a few angles [11]. Provided that the gantry has a sufficiently large number of coils (e.g. 8 or more),restricting beam delivery only to discrete angles is not a true limitation.

The N coils of each toroid do not need to be equally spaced in the θ angle. In fact, as we will show later in Section 3.2.4, it is beneficial to group coils in pairs, thus decreasing peak field in the coil for a given bending strength, as well as lowering the inductance and stored magnetic energy of the system.

The shape of the area of magnetic field, and the dependency of field on position, and in particular on the radius, is the result of the selected coil geometry. In the absence of magnetic materials, not considered in this paper, this is a linear dependency on the position of the conductors. It is in particular interesting to *grade* the coil by spacing the winding so to obtain the required field index n introduced earlier Eq. (5). We expand more in detail on the coil shape and coil grading in the following sections.

Finally, we mentioned earlier that the gantry may consist of a sequence of co-axial toroids. Equivalent to what is done alternating quadrupole gradients in a transfer line, we could imagine a sequence of two toroids, the first with negative field index $n < 0$, followed by one

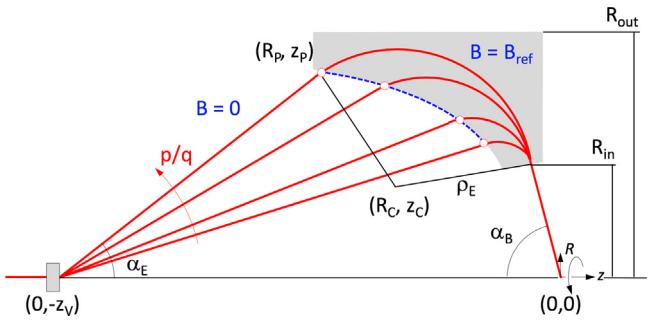

Fig. 8. Construction of the ideal profile of a toroidal field boundary that focuses particles of different momentum to charge ratio p/q on a single focal point by making use of different kick angles at the location of the vector magnet. The toroidal field area is shaded in the picture. The dashed boundary can be computed using Eq. (10) or Eq. (11).

with positive field index $n > 0$. The first would be the equivalent of a defocusing quadrupole, the second one would be a focusing quadrupole. It should then be possible to design the single toroids for strength, field index, length and position that achieve optimal field transfer. Nonetheless, as we will show later, satisfactory results can be achieved already with a single toroidal magnet. This is why the analysis and discussion below is limited to the case of a single toroid, and we reserve the idea of several toroids for future development.

3.2.1. Coil geometry

We address here the question of the optimal coil shape to achieve perfect iso-centric conditions for particles of different momentum to charge ratio. The toroidal magnet receives a particle bent to an arbitrary angle by the vector magnet placed at coordinates $(0,-z_V)$. We wish to find the coil shape that focuses the particles in the origin of the reference frame (0,0), with the additional constraint that the particles must impinge with a constant angle α_B. This situation is shown schematically in Fig. 8. A particular case is obtained when the impinging beam angle is normal to the z-axis (patient), i.e. $\alpha_B = 90$ degrees, as is customary in gantries built with rotating beamlines. This is not a constraint in our case.

For the field profile, we make the assumption that the winding is graded so to generate a constant field $B_\theta = B_{ref}$ (i.e. $n = 0$ in Eq. (5), see later discussion on grading) and that the coil boundary corresponds to a hard edge, i.e. zero field outside the winding. These are rather ideal conditions, but have the benefit to yield a closed analytic solution and provide a good starting point for a magnet shape optimization based on numerical analysis. Similar work done in the past to design toroidal lenses, considering the ideal $1/R$ dependency of the field, required numerical solution [27].

Based on the above assumptions, and with the notation indicated in Fig. 8, it is possible to use simple geometric relations and trace the particle trajectory backward, starting from the point (0,0) towards its origin $(0,-z_V)$. The beam travels in a cone of angle α_B first, until it enters the toroidal field area at a radius R_{in}. Once in the toroidal field, the trajectory is a circumference with radius (see Eq. (2)):

$$\rho_E = \frac{p}{qB_{ref}} \tag{6}$$

The circumference portion of the trajectory, corresponding to the extension of the field area, needs to terminate at the location (R_P, z_P) where the tangent points to the vector magnet. The center of the bent particle trajectory in the field area is given by:

$$R_C = R_{in} - \rho_E cos\left(\alpha_B\right) \tag{7}$$

$$z_C = \frac{R_{in}}{tg\left(\alpha_B\right)} + \rho_E sin\left(\alpha_B\right) \tag{8}$$

and the angle corresponding to the optimal direction of the particle α_E can be computed as follows:

$$\alpha_E = arcsin\left(\frac{\rho_E\left(z_V - z_C\right) + R_C\sqrt{R_c^2 + z_V^2 - \rho_E^2}}{R_C^2 + \left(z_V - z_C\right)^2}\right) \tag{9}$$

Given a range of momentum to charge (e.g. 1.2 Tm to 2.4 Tm for protons), the toroidal field B_{ref}, the inner radius R_{in}, a desired incident angle α_B and the location of the vector magnet z_V it is possible to use the above equations parametrically to determine the curvature radius ρ_E, the center of the particle trajectory (R_C, z_C) and the vector angle α_E for each value of p/q. Having computed these quantities, it is finally possible to reconstruct the locus of the points (R_P, z_P), i.e. the entry profile of the field area, which, based on our assumptions, is identical to the coil profile. This is given by:

$$R_P = R_C + \rho_E cos\left(\alpha_E\right) \tag{10}$$

$$z_P = -z_C - \rho_E sin\left(\alpha_E\right) \tag{11}$$

Fig. 9 shows the vector angle and the ideal coil profile computed for a proton gantry, with a field of $B_{ref} = 3$ T, an inner radius R_{in} of 0.4 m, an incident angle α_B of 90 degrees and a vector magnet located at $z_V = 4$ m, reasonably far away from the toroidal magnet to limit the required strength and aperture, but still maintain a compact installation. The bending radius for the maximum energy considered, 250 MeV, is $\rho_E = 0.8$ m. The outer radius will be in the range of 1.2 m, which is very compact. To be noted that the magnet bore, 0.8 m, has been chosen intentionally small, in the range of that of MRI magnets, to find the minimal possible dimension that can be achieved with one such system. We are aware that this does not leave enough room to insert the customary beam diagnostics and controls. Indeed, adding the typical dimension of a radiation therapy *nozzle* would at least double the magnet bore. It is however interesting to note at this point that work is in progress to examine the possibility to integrate compact solid-state beam range and position monitoring in the gantry dimension assumed here [28].

Using the analytical results, and with the choice of parameters above the coil contour is nearly straight, and the angle dependence on the kinetic energy of the beam is also approximately linear. Though not essential, these features offer the benefit of easy coil winding, and simple operation. A final remark is that if the position of the vector magnet is sufficiently far from the gantry, Eq. (9) can be simplified to the trivial expression:

$$\alpha_E \approx \frac{R_{in} + \rho_E}{z_V - \rho_E} \tag{12}$$

These simple expressions give an ideal solution that can be used as a starting point for further optimization.

As reported in Fig. 9, the required kick for the highest momentum is about 30 degrees. The corresponding clear aperture for a vector magnet with a length of 1 m would then be 50 cm, i.e. very large. As discussed earlier this shows that this element of the system requires innovative solutions.

3.2.2. Grading in radial direction

The field dependence on the radius, which we expect to be one of the main characteristics affecting beam transport, can be adjusted by *grading* the coil winding. The basic idea of grading is to extend the radial build of the coils, which so far were assumed to have infinitesimal thickness. By spacing the conductors in the winding, we can distribute the current density and modify the natural field dependence of the ideal torus, Eq. (1), to achieve a desirable shape, e.g. Eq. (5). In the toroidal gantry configuration we can allow ourselves unconstrained grading in the coil cross section, i.e. filling the whole space of a coil, without affecting the space available for the beam passage.

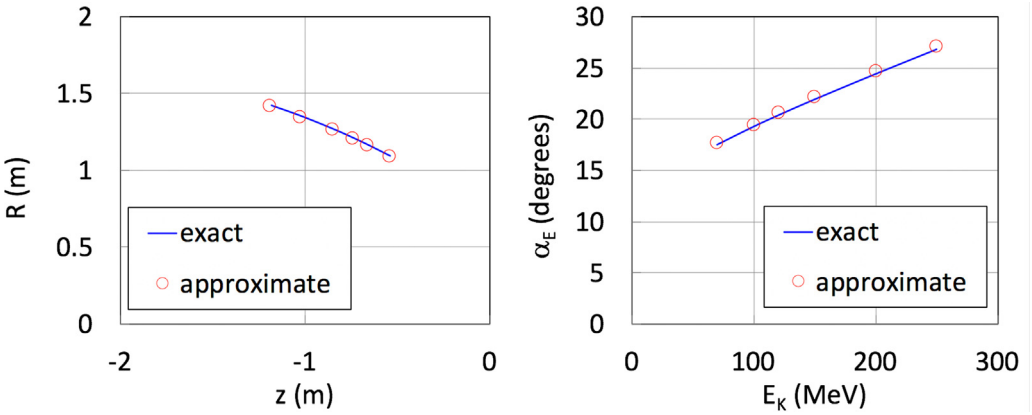

Fig. 9. Ideal inboard coil winding profile (left) and optimal angle given by the vector magnet (right) to obtain iso-centric focusing of proton beams of different kinetic energy in the range 70 MeV to 250 MeV, using the exact expression Eq. (9), and the approximation Eq. (12).

To show the principle of grading we take the ideal axis-symmetric torus, with an *inboard* (small radius) and *outboard* (large radius) windings of finite thickness, providing the main part of the toroidal field. The inboard leg extends from $R = R_{in}$ (the inner magnet bore radius) to $R = R_0$, and the outboard leg spans from $R = R_1$ to $R = R_{out}$ (the outer radius of the torus magnet). We assume for simplicity that the two legs have constant current density J_W. The space between inboard and outboard legs (i.e. $R_0 < R < R_1$) contains windings with an average current density $J(R)$. This situation is shown schematically in Fig. 10.

Using induction circulation theorem:

$$B_\theta(R) = \frac{\mu_0 I(R)}{2\pi R} \tag{13}$$

we can find the field current distribution that produces a desired field profile, such as Eq. (5). After some simple algebra, the complete solution for the field and current density, including the ideal toroidal field generated in the inboard and outboard legs, is:

$$B_\theta^{graded}(R) = \begin{cases} \frac{\mu_0 J_W}{2}\left(R - \frac{R_{in}^2}{R}\right) & R_{in} \le R \le R_0 \\ \frac{B_{ref} R_{ref}^n}{R^n} & R_0 \le R \le R_1 \\ \frac{B_{ref} R_{ref}^n}{R_1^n R} + \frac{\mu_0 J_W}{2}\left(R - \frac{R_1^2}{R}\right) & R_1 \le R \le R_{out} \end{cases} \tag{14}$$

$$J(R) = \begin{cases} J_W & R_{in} \le R \le R_0 \\ \frac{1-n}{\mu_0}\frac{B_{ref} R_{ref}^n}{R^{n+1}} & R_0 \le R \le R_1 \\ -J_W & R_1 \le R \le R_{out} \end{cases} \tag{15}$$

We see from Eq. (14) that it is indeed possible to achieve any desired field index by acting on the current distribution as from Eq. (15). As an example, a choice of $n = 0$, which corresponds to a constant field in the magnet bore, is produced by a current density with a $1/R$ dependency in the space between inboard and outboard legs. The corresponding current density and field profile are plotted in Fig. 10. Another interesting case is n=–1, which corresponds to a constant current density in the space between inboard and outboard legs, and produces an ideal radial field gradient, with field increasing proportionally to the radius. Such field could be useful in a sequence of tori with alternating radial gradients. Though the above solutions are only ideal, they give guidelines on how to space conductors in a practical winding so to adjust the field towards a desired optimum value.

3.2.3. Discrete coils — uniform spacing

In our analysis towards a realistic system we need to consider that the toroidal magnet is built using discrete coils. Besides being a practical solution for the construction of the magnet, the toroidal magnet must be built with coils to ensure that there is a free space for the beam passage. In a torus of discrete coils, the field deviates from the ideal case considered so far. Specifically, for a set of discrete coils the field is no longer axis-symmetric, though it remains periodic, and its strength varies depending on the toroidal angle θ.

To quantify this effect and derive guidelines on the number of coils to be used in a practical system, we use the method developed in [29], based on the calculation of the field generated by a torus of filamentary and planar coils with large elongation. This situation is shown schematically in Fig. 11 (left), which shows the intersection of the inboard and outboard legs of N discrete filamentary coils with the plane $z = 0$. The extension of the coils along the z-axis is considered as infinite. In a first instance the coils are considered as uniformly spaced in angle. As shown in [29], the field generated by this configuration is given by:

$$B_\theta^{discrete}(R,\theta) = \frac{\mu_0 N I}{2\pi R}\left[\left(1 - \frac{1-\rho_{in}\cos(n\theta)}{1-2\rho_{in}\cos(n\theta)+\rho_{in}^2}\right) - \frac{\rho_{out}^2 - \rho_{out}\cos(n\theta)}{1-2\rho_{out}\cos(n\theta)+\rho_{out}^2}\right] \tag{16}$$

where we have used the following definitions:

$$\rho_{in} = \left(\frac{R}{R_{in}}\right)^N \tag{17}$$

$$\rho_{out} = \left(\frac{R}{R_{out}}\right)^N \tag{18}$$

We can compute the field given by Eq. (16) at various toroidal angles, and in particular the angle corresponding to the coil plane (i.e. $\theta = \pi/N$ in Fig. 11) and the angle corresponding to the plane in the middle of two neighboring coils (i.e. $\theta = 0$ in Fig. 11). An inner radius of $R_{in} = 0.4$ m and outer radius of $R_{out} = 1.6$ m have been taken for this evaluation, and the current has been computed to obtain in the ideal case a reference field of $B_{ref} = 3$ T at a reference radius corresponding to the average radius of the toroid, $R_{ref} = 1$ m. The toroidal field values obtained by this method are compared in Fig. 12 to the ideal toroidal field that corresponds to the axis-symmetric configuration and identical total amperage, taking as a parameter the number of coils N. We see, as expected, that the toroidal field in the coil plane is higher than the ideal case, and in contrast the field in the plane cutting the space between two coils is lower. Note that due to the filamentary assumption the field diverges in the coil plane, when approaching the filament location. The value of the ideal toroidal field is bracketed by the two values obtained in the coil plane and the inter-coil midplane.

It is evident from the results reported in Fig. 12 that the peak field in the coil is significantly higher than the desired field strength in the beam passage, where we can take the reference radius as a representative location. This is due not only to the radial dependence

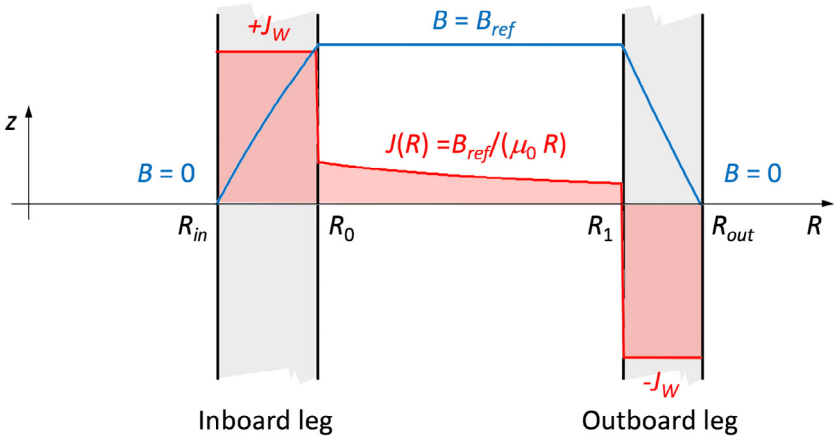

Fig. 10. Schematic current distribution and resulting field profile as a function of radius in an ideal torus with graded winding, showing the location and extension of the inboard and outboard winding legs. The case of a field index $n = 0$ (constant field) is shown as an example.

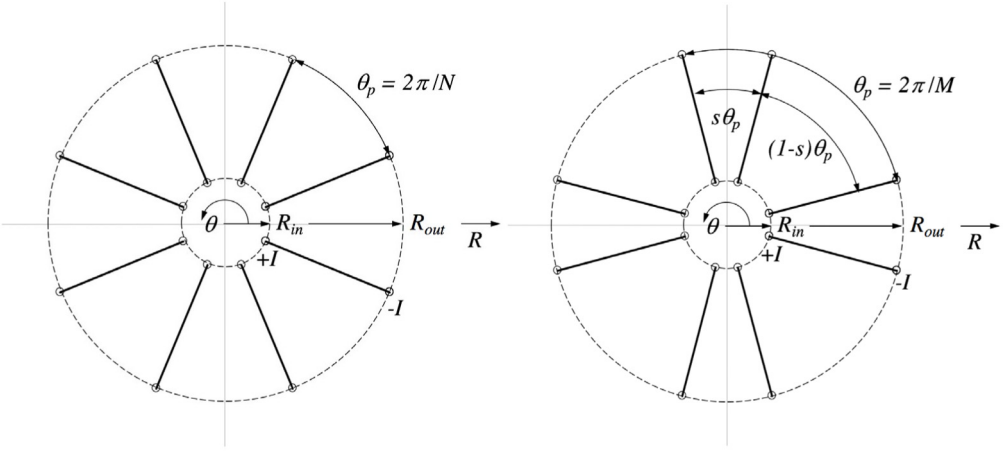

Fig. 11. Schematic representation of the configuration used to compute the field produced by N discrete filamentary coils of large elongation (infinite extension in z), showing the intersection of the filamentary inboard and outboard coil limbs with the $z = 0$ plane (circles). Two configurations are shown: uniformly spaced coils in the angle q (left) and non-uniformly spaced coils (right). The number of coils is $N = 8$ in the example above, grouped in $M = 4$ coil pairs for non-uniformly spaced coils.

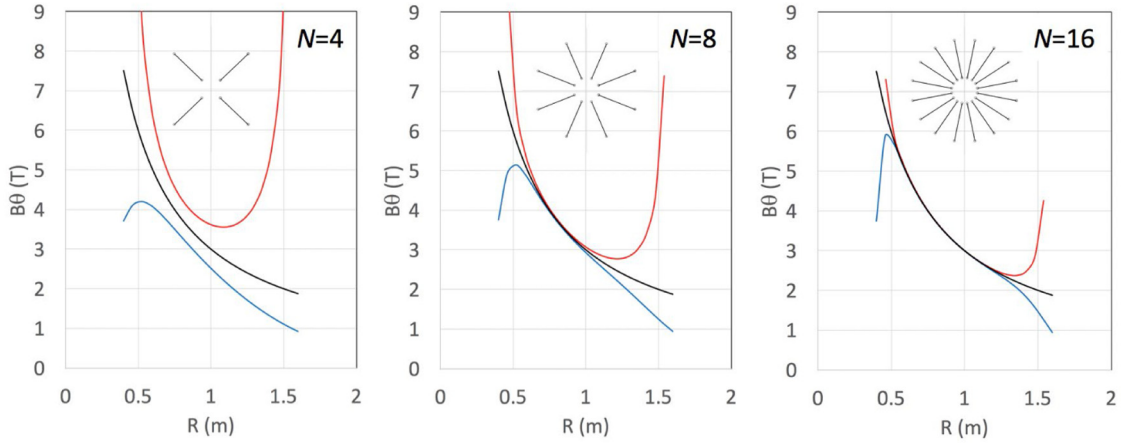

Fig. 12. Comparison of toroidal field values computed in the two planes at $\theta = 0$ (beam passage, blue line) and $\theta = \pi/N$ (coil, red line) using the discrete coils approximation of Eq. (16). The ideal field dependence obtained from Eq. (1) is also reported for comparison (black line). (For interpretation of the references to color in this figure legend, the reader is referred to the web version of this article.)

of the ideal toroidal field, but also to the deviation from the ideal profile due to the discrete coils. In order to quantify this effect, we can define a *field ratio* f that measures the effectiveness of the discrete coil configuration when compared to the ideal toroidal field profile:

$$f = \frac{B_\theta^{discrete}\left(R_0, \pi/N\right)}{B_\theta^{discrete}\left(R_{avg}, 0\right)} \frac{R_0}{R_{avg}} \tag{19}$$

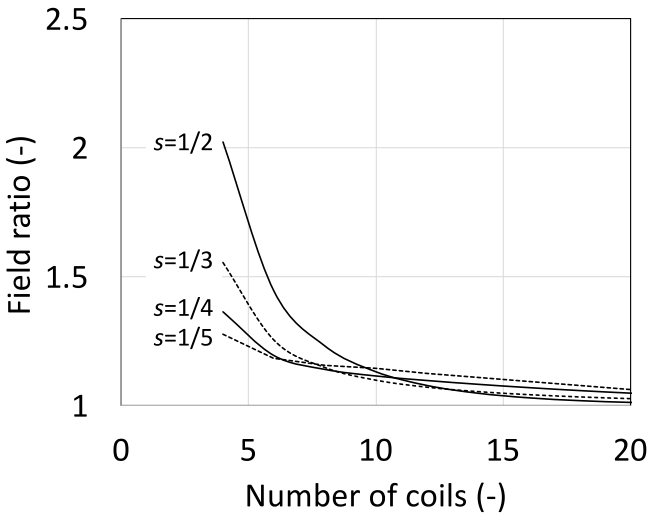

Fig. 13. Field ratio f as defined in Eq. (19), measuring the amplification of the peak field in the winding of discrete coils with respect to the ideal toroidal field profile, plotted as a function of the total number of coils N. Different configurations are reported, equally spaced discrete coils (s=1/2), as well as non-equally spaced coils with different spacing (s=1/3, s=1/4, and s=1/5).

The above ratio gives an estimate of how much the desired bending field, i.e. in the beam plane and at the representative radial location R_{avg}, is *amplified* at the coil peak field location, i.e. in the coil plane and at the inboard coil leg. To avoid the singularity in the field evaluation of Eq. (19), the peak field is evaluated at the radial location R_0 as defined in Fig. 10, i.e. the maximum radial extension of the inboard leg of the coil. Finally, note that we have constructed the ratio of Eq. (19) to compensate for the $1/R$ dependence of the ideal toroidal field (through the ratio of radii in the second fraction), so that to first order we can assume that f does not depend on coil grading and the associated deviation from the ideal $1/R$ dependence.

We can now use the definition Eq. (19) to evaluate the field ratio as a function of the number of coils N composing the torus, in Fig. 13. For this evaluation we assume the same geometry used earlier, and we take a tentative coil thickness of 0.1 m (consistent with the proton gantry design described later), resulting in a value of $R_0 = 0.5$ m. The field ratio is significantly larger than one when the torus is composed of only a few coils (i.e. below ten for our choice of parameters), and approaches one once the number of coils increases. Taking as an example the extreme case of a torus made of four coils, the peak field is evaluated to be twice as high as would be obtained from the ideal field dependence. The ideal dependence of the toroidal field on radius is R_{ref}/R_0, which in our case is also a factor two (see values used above). So, in this extreme choice of parameters, the coil would experience a field four times higher than the reference field at R_{ref}.

3.2.4. Discrete coils — non-uniform spacing

In principle, a torus can be assembled also as a set of periodic but non-uniformly spaced coils. An example of this situation is shown in Fig. 11(right), where N coils are grouped in M pairs with a given angle opening. The pairs are periodically spaced along the angle θ, with a period $\theta_p = 2\pi/M$. We quantify the coil spacing in a pair by using a parameter s such that the angle between the coils in a pair is given by $s\,\theta_p$ (see Fig. 11), with $0 < s \leq 0.5$. We expect the field to increase in the space between two coils of a pair, which is where the beam will pass. This configuration, made of N coils, results in $M = N/2$ identical beam channels.

The field produced by this configuration can be computed using Eq. (16), considering two groups of M equally spaced coils, and adding their field contributions. Using this simple expedient, we can repeat the analysis performed above, in the case of uniformly spaced coils. The field profiles of a toroidal magnet with $R_{in} = 0.4$ m, $R_{out} = 1.6$ m and 3 T field at $R_{fref} = 1$ m are reported in Fig. 14, to be compared to the analogous calculation reported in Fig. 12. For this sample evaluation we have taken a coil spacing $s = 1/5$. We note that the coil grouping in pairs has the expected effect of increasing both the field in the space traversed by the beam, as well as the peak field. The effect is more pronounced for a low number of coils, which is also expected. In principle, this configuration produces hence a higher field than a toroid of uniformly spaced coils.

To quantify the benefit, we have repeated the calculation of the field factor defined in Eq. (19) for the above geometry, and various values of the coil spacing s. The results are shown in Fig. 13 already discussed earlier. We note that the field factor decreases significantly at decreasing s when the number of coils is small, i.e. below 10 for our choice of torus geometry. The gain is appreciable, e.g. for four coils the peak field is reduced from twice larger than in the ideal torus, for equally spaced coils, to only 20% larger if a spacing of $s = 1/5$ is taken. At the same time, when the number of coils increases, we see that there is no benefit in the configuration with non-uniform spaced coils. The reason is that although the field in the beam space is higher for non-uniform spacing, the peak field is also increased by the proximity of the coils at the inboard leg. For a large number of coils, in any case, the field approaches very closely that of the ideal toroid, i.e. $f \approx 1$. We remark finally that the bore radius of the toroid R_{in} also has a strong impact on these results, where the benefit of non-uniform spacing increases for tori of increasing dimension, since the azimuthal coil distance at R_{out} relative to that at R_{in} differs relatively less if the radius of the toroid is large.

3.2.5. Force and energy scaling

As a last element in this summary of the cardinal properties of a toroidal magnet, it is interesting to report basic estimates for the forces acting on the coil, and the stored energy. We limit our discussion to the case of an ideal circular torus, and we use the results of [29], suitably rearranged.

The only net force that the coil experiences is in radial direction, and is given by:

$$F_R = -\frac{2\pi^2 R_{ref}^2 B_{ref}^2}{\mu_0 N}\left(1 - \frac{1}{\sqrt{1-\gamma^2}}\right) \tag{20}$$

which is a centering force (note the negative sign). The coil also experiences internal forces that have zero resultant but produce internal stress in the coil. The force in z direction on the upper half of the coil, representative of the level of internal forces, is given by:

$$F_z = \frac{\pi R_{ref}^2 B_{ref}^2}{\mu_0 N} ln\left(\frac{1+\gamma}{1-\gamma}\right) \tag{21}$$

Above we have defined γ as the ratio of the minor to major ratio, obtained as follows:

$$\gamma = \frac{R_{out} - R_{in}}{R_{out} + R_{in}} \tag{22}$$

From Eqs. (20) and (21) the forces per coil of a torus of given aspect ratio are proportional to the square of the desired toroidal field B_{ref}, and the square of the reference radius R_{ref}. Considering a coil of given geometry and bending power (i.e. at fixed B_{ref}) from the scaling above we see that it is hence advantageous to have the toroid as small as possible.

To compute the stored energy we use the expression of the inductance of an ideal circular torus [29]:

$$L = \mu_0 N^2 \frac{R_{in} + R_{out}}{2}\left(1 - \sqrt{1-\gamma^2}\right) \tag{23}$$

and obtain:

$$E = \frac{1}{2} L I^2 = 4\pi^2 \frac{R_{ref}^2 B_{ref}^2}{2\mu_0} \frac{R_{in} + R_{out}}{2}\left(1 - \sqrt{1-\gamma^2}\right) \tag{24}$$

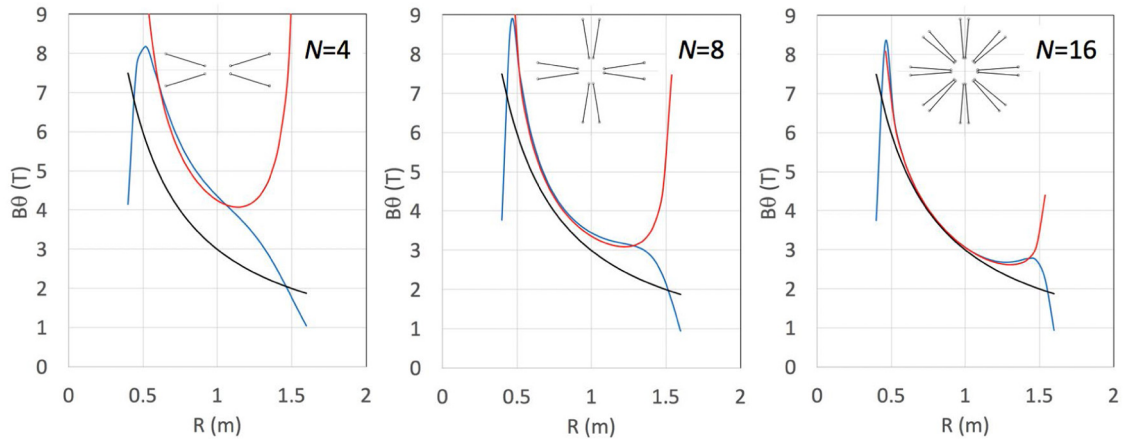

Fig. 14. Comparison of toroidal field values computed in the two planes at $\theta = 0$ (beam passage, blue line) and $\theta = s\ \pi/M$ (coil, red line) for a configuration consisting of non-uniformly spaced N coils grouped in M pairs, with $s = 1/5$. The ideal field dependence obtained from Eq. (1) is also reported for comparison (black line). (For interpretation of the references to color in this figure legend, the reader is referred to the web version of this article.)

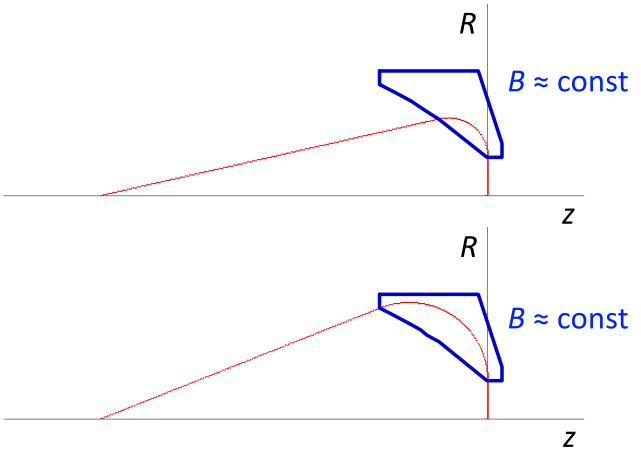

Fig. 15. Ideal toroidal field coil shape used as initial guess for the optimization of the coil geometry, and sample demonstration of iso-centric focusing obtained tracking proton beams of different kinetic energy of 70 MeV (top) and 250 MeV (bottom). The field is assumed to be constant (graded windings) in the coil area.

In this case the stored energy of a torus of given aspect ratio increases with the square of the reference field B_{ref}, and with the approximate third power of the radius R_{ref}. Here again, we see the advantage of keeping the radius of the torus as small as possible, compatibly with field and geometry requirements. Given the approximate scaling law established in [30] for the cost of a superconducting magnet system, and in particular its proportionality to the square root of the stored energy, we expect that the cost of the toroidal gantry will scale like:

$$C \approx \sqrt{E} \propto B_{ref} R_{ref}^{\frac{3}{2}} \tag{25}$$

According to Eq. (25), the radial dimension of the toroidal magnet has a stronger influence than the field, supporting analytically the intuitive desire to optimize the magnet design for the smallest possible radius compatibly with the operating margin of the superconducting coil.

While useful in providing general trends, it is clear that the above scaling, based on a much simplified geometry, will tend to fail when considering real magnet features. One specific feature is that in the energy and cost scaling above we see no dependency on the number of coils, which is inherent to the assumption of an ideal toroid. Scoping studies have shown that this is no longer true when considering toroids of very large dimension, built with discrete coils non-equally spaced,

Table 1
Main parameters of the proton gantry described in the text.

Energy range	[MeV]	70…250
Number of coils	[–]	16
Torus inner diameter	[m]	0.8
Torus outer diameter	[m]	3.3
Torus length	[m]	1.8
Effective field	[T]	~3
Peak field	[T]	8.2
Stored magnetic energy	[MJ]	34
Magnet mass	[tons]	12

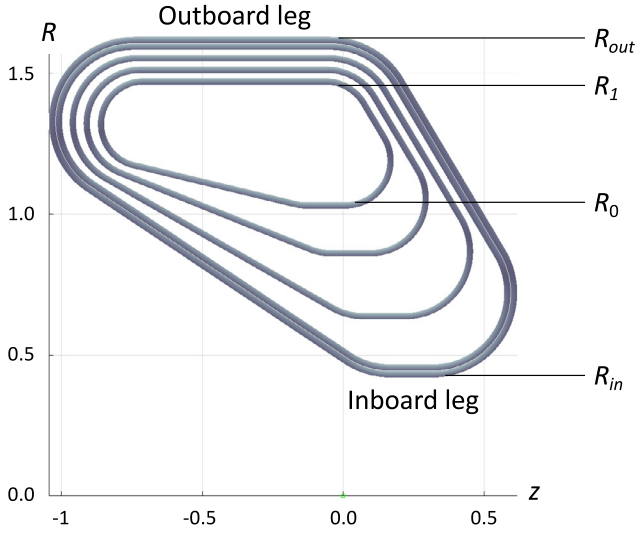

Fig. 16. Optimized coil geometry for a proton gantry.

grouped to provide discrete beam channels as discussed earlier [31]. In this case the cost becomes proportional to the number of coils (i.e. the number of beam delivery directions), while the dependency from the radius becomes very weak. This is a different *design point* with respect to the compact concept described here, which we do not explore further in this paper.

4. Toroidal magnet design example

Drawing from the considerations in the previous section, and assuming the same parameters used so far, we show here the design

Fig. 17. *Front* (beam side, left) and *back* (patient side, right) view of the complete toroidal magnet for a proton gantry, with inner bore diameter of 0.8 m. Outer dimension is a diameter of 3.3 m, including the concept of support structure.

of a toroidal magnet with the desired characteristics of a gantry. The example is for a proton beam with energy range of 70 MeV to 250 MeV. The same design principle applies to any p/q ratio, and specifically to a carbon ion gantry provided the combination of size and magnetic field is scaled by the ratio of rigidity (approximately 2.7).

The coil shape and grading are determined by a numerical optimization of the conductor positions, based on a magneto-static calculation and particle tracking, to achieve isocentric conditions in the whole range of energy considered [25,32]. As a starting point for this optimization we take the ideal contour of the toroidal coil leg at the entrance of the beam as computed in Fig. 9, i.e. for a constant toroidal field (field index $n = 0$). The complete coil contour is then obtained extending the beam entrance profile to the inner radius, and adding an arbitrary return leg, shaped to reduce the field volume (simple straight lines). This schematic ideal coil shape is reported in Fig. 15, where we also demonstrate that the two beams at the extreme of the beam energy range considered, i.e. 70 MeV and 250 MeV, behave as expected.

To obtain the actual design of the toroidal magnet we then built discrete, graded coils of finite dimensions, initially shaped as in Fig. 15. For this study we have taken a total of $N = 16$ coils, each coil consisting of 5 grades. The selection on the number of coils was based on the considerations of field homogeneity and peak field (see discussion above), while the choice of the number of grades was driven by computational time. The coil geometry was parametrized for the numerical optimization, inserting feasible bending radii, and the curved region required by Eqs. (9) and (10) was substituted by a straight part for simplicity (this is close enough to the profile shown in Fig. 9). The optimization was then run to obtain suitable spacing among grades, and achieve the desired beam bending properties with the lowest peak field on the winding.

The result of this exercise is shown in Fig. 16, representing the geometry of a single coil, and Fig. 17, reporting schematically the full torus of 16 coils, including the concept of support structure. The final result of the optimization is a field shape that deviates from the ideal field index $n = 0$ assumed at the start, which is necessary as the winding is discrete and finite in dimension.

The main features of the magnetic system are summarized in Table 1. The 5 grades of the optimized coil have of equal number of turns, and we foresee to wind the coil as a double pancake. Once assembled the torus has an outer diameter of 3.3 m and a length of 1.8 m. The peak field on the conductor is 8.2 T, i.e. suitable for Nb–Ti. The magnet, together with the mechanical structure, has a mass of 12 tons, and stores an energy of 34 MJ. These are very modest parameters if compared to the typical mass of conventional gantries. As we remarked earlier, this is mainly the result of the choice of a small magnet bore (0.8 m), as typical of MRI magnets. One such gantry system would be feasible only with significant advances in beam range and position monitoring [Bot-2020]. It is nonetheless an interesting exercise to provide the lower limit of dimension and mass of the toroid as a benchmark for the selection of different design parameters. Further details as to the engineering performance of this design can be found in [32].

5. Conclusions and perspectives

The concept of a toroidal magnet discussed in this paper appears to offer an interesting alternative to the present state-of-the-art design of gantries for hadron therapy. The magnet has a large acceptance, and does not need to turn, eliminating in principle the need for massive structures and high-precision mechanics. Furthermore, the static and axis-symmetric configuration is well suited to the use of a superconducting winding, with the potential of considerable reduction in size. Provided the magnet technology can be kept simple, which requires a detailed optimization and engineering design, it can be envisaged to significantly reduce the size of gantries, possibly to the scale of a few meters linear dimension and masses of the order of ten tons (protons) to a few tens of tons (ions).

A number of key issues need to be addressed to advance the concept described in this paper to the next level of engineering design. High priority is required for the formalization of beam transport through toroidal fields of various index and curvature, possibly using analytical methods and approximations that could guide the design of the optimal field configuration. In relation to the above point, an analytical expansion of the magnetic field generated by a coil with given geometry will be required to produce an optimum magnet design, along the lines described in [33].

All aspects of superconducting magnet design also need to be considered in detail, i.e. material and conductor selection, operating temperature and margin, operating current and voltage, circuit topology, quench detection and protection strategy. The simple mechanical concept needs to be translated into the design of a supporting structure that withstands nominal and off-nominal load conditions (e.g. quench or magnet failure), and is compatible with the required beam line geometry. Finally, vacuum, cryogenics and beam monitoring aspects

need to be addressed and integrated in the design. The concept needs to be validated in a demonstration set-up, and we are realizing a scaled-down version of a single-coil, to be tested, possibly in a magnetic mirror configuration, which will provide a proof of technological feasibility.

Finally, the second element of the beam delivery of this toroidal gantry, the vector magnet, needs to be developed beyond the simplified concept of a point source. In this paper, we have only listed options and issues, which we plan to address in the future and arrive to a feasible magnet configuration.

CRediT authorship contribution statement

L. Bottura: Conceptualization, Methodology, Writing - original draft, Visualization, Project administration, Funding acquisition. **E. Felcini:** Methodology, Software, Validation, Investigation, Writing - review and editing, Visualization. **G. De Rijk:** Supervision, Project administration, Funding acquisition. **B. Dutoit:** Supervision.

Declaration of competing interest

The authors declare that they have no known competing financial interests or personal relationships that could have appeared to influence the work reported in this paper.

Acknowledgment

The work reported in this paper is supported by the Budget for Knowledge Transfer to Medical Applications of the European Organization for Nuclear Research (CERN), Geneva, Switzerland.

References

[1] G. Kraft, The radiobiological and physical basis for radiotherapy with protons and heavier ions, Strahlenther. Onkol. 166 (1) (1990) 10–13.
[2] H. Tsujii, et al., Clinical results of carbon ion radiotherapy at NIRS, J. Radiat. Res. 48 (Suppl.) (2007) A1–A13.
[3] H. Tsujii, T. Kamada, T. Shirai, K. Noda, H. Tsuji, K. Karasawa (Eds.), Carbon-Ion Radiotherapy: Principles, Practices, and Treatment Planning, Springer, Japan, 2014.
[4] M. Durante, R. Orecchia, J.S. Loeffler, Charged-particle therapy in cancer: clinical uses and future perspectives, Nature Rev. Clin. Oncol. 14 (8) (2017) 483–495.
[5] K. Takada, Qualitative comparison of proton beams and other radiotherapy beams, in: K. Tsuboi, T. Sakae, A. Gerelchuluun (Eds.), Proton Beam Radiotherapy, Springer, Singapore, 2020.
[6] A. Degiovanni, U. Amaldi, History of hadron therapy accelerators, Phys. Med. 31 (2015) 322–332.
[7] J.M. Schippers, A. Lomax, A. Garonna, K. Parodi, Can technological improvements reduce the cost of proton radiation therapy?, Semin. Radiat. Oncol. C 28 (2018) 150–159.
[8] U. Amaldi, et al., Accelerators for hadron therapy: from Lawrence cyclotrons to Linacs, Nucl. Instrum. Methods A 620 (2010) 563–577.
[9] U. Weinrich, Gantry design for proton and carbon hadrontherapy facilities, in: Proc. EPAC 2006, Edinburgh, Scotland, 2006, pp. 964–968.
[10] H. Owen, A. Lomax, S. Jolly, Current and future accelerator technologies for charged particle therapy, Nucl. Instrum. Methods A 809 (2016) 96–104.
[11] S. Yan, et al., Reassessment of the necessity of the proton gantry: Analysis of beam orientations from 4332 treatments at the massachusetts general hospital proton center over thepast 10 years, Int. J. Rad. Oncol. Biol. Phys. 95 (1) (2016) 224–233.
[12] S. Rossi, The national centre for oncological hadrontherapy (CNAO): Status and perspectives, Phys. Med. 31 (2015) 333–351.
[13] E. Pedroni, et al., The 220-MeV proton therapy project at the Paul Scherrer Institute: Conceptual design and practical realization, Med. Phys. 22 (1) (1995).
[14] R. Fuchs, U. Weinrich, P. Emde, The heavy ion gantry of the HICAT facility, in: Proc. EPAC 2004, Lucerne, Switzerland, 2004, pp. 2550–2552.
[15] Y. Iwata, K. Noda, T. Shirai, et al., Design of a superconducting rotating-gantry for heavy-ion therapy, Phys. Rev. ST Accel. Beams. 15 (2012) 044701.
[16] D. Trbojevic, Carbon/proton therapy: A novel gantry design, Phys. Rev. Spec. Top. - Accel. Beams 10 (2007) 053503.
[17] A. Gerbershagen, A novel beam optics concept in a particle therapy gantry utilizing the advantages of superconducting magnets, Z. Med. Phys. 26 (2016) 224–237.
[18] Y. Iwata, et al., Development of curved combined-function superconducting magnets for a heavy-ion rotating-gantry, IEEE Trans. Appl. Superconduct. 24 (3) (2014).
[19] D.S. Robin, et al., Superconducting toroidal combined-function magnet for a compact ion beam cancer therapy gantry, Nucl. Instrum. Methods Phys. Res. A 659 (2011) 484–493.
[20] W. Wan, Alternating-gradient canted cosine theta superconducting magnets for future compact proton gantries, Phys. Rev. ST Accel. Beams 18 (2015) 103501.
[21] L. Bromberg, Toroidal Bending Magnets for Hadron Therapy Gantries, US9711254B2, 2016.
[22] V. Lante, et al., ULICE Deliverable Report JRA6.3: Conceptual Design of a Carbon Ion Gantry, 2009.
[23] D. Boyd, H.A. Schwettman, J. Simpson, Large acceptance pion channel for cancer therapy, Nucl. Instrum. Methods 111 (1973) 315–331.
[24] I. Horvath, G. Vecsey, J. Zellweger, The piotron at sin - A large superconducting double torus spectrometer, IEEE Trans. Magn. MAG-17 (5) (1981).
[25] E. Felcini, L. Bottura, J. van Nugteren, A. Gerbershagen, Particle tracking and beam optics analysis on toroidal gantry for hadron therapy, Focus Early Career Res. Phys. Med. Biol. (2020) unpublished.
[26] A Gantry and Apparatus and Apparatus for Focussing Beams of Charged Particles, European Patent Application EP3573075, 27 2019.
[27] A. Mohri, K. Ikuta, J. Fujita, New lens system using toroidal magnetic field for intense ion beam, Japan. J. Appl. Phys. 16 (3) (1977) 491.
[28] L. Bottura, E. Felcini, V. Ferrero, E. Fiorina, V. Monaco, F. Pennazio, G. de Rijk, P. Cerello, Delivery, beam and range monitoring in particle therapy in a highly innovative integrated design, Front. Phys. Med. Phys. Imaging (2020) unpublished.
[29] J.M. Thome, R.J. Tarrh, MHD and Fusion Magnets Fusion Magnets, John Wiley & Sons, Inc, 1982.
[30] M.A. Green, B.P. Strauss, The cost of superconducting magnets as a function of stored energy and design magnetic induction times the field volume, IEEE Trans. Appl. Supercond. 18 (2) (2008).
[31] A. Louzguiti, Private Communication, 2019, also available at https://indico.cern.ch/event/848512/.
[32] E. Felcini, L. Bottura, J. van Nugteren, G. de Rijk, G. Kirby, B. Dutoit, Magnetic design of a superconducting toroidal gantry for hadron therapy, IEEE Trans. Appl. Supercond. 30 (4) (2020).
[33] L. Gambini, M. Breschi, E. Felcini, A. Cristofolini, L. Bottura, An algorithm for toroidal field harmonics computation in arbitrary magnetic configurations, IEEE Trans. Appl. Supercond. 30 (4) (2020).